Influence of carbon, manganese and nickel on microstructure and properties of strong steel weld metals
Part 2 – Impact toughness gain resulting from manganese reductions

E. Keehan*[1], L. Karlsson[2], H.-O. Andrén[3] and H. K. D. H. Bhadeshia[4]

Two experimental high strength steel weld metals were produced with 7 wt-% nickel and either 2 or 0·5 wt-% manganese. Neural network predictions that it is advantageous to reduce the manganese concentration in high nickel alloys have been confirmed, with impact energy increasing from 32 to 113 J at –40°C. High resolution microstructural investigations showed that both weld metals contained mainly martensite at interdendritic regions and predominantly bainite at dendrite core regions, as a consequence of manganese and nickel segregation. In the high manganese weld metal significant amounts of coarse grained coalesced bainite formed whereas mainly upper bainite was seen with 0·5 wt-% manganese. Reducing manganese content increased the transformation temperature, promoting fine upper bainite at the expense of coarse coalesced bainite. Increased toughness was attributed to the finer grain size of bainite constituents and a more effectively tempered microstructure.

Keywords: High strength steel weld metal, Nickel content, Manganese content, Impact energy, Microstructure, Martensite, Bainite, Segregation, Coalesced bainite, Toughness

Background

High strength steel is increasingly employed in greater amounts owing to the many advantages it offers, such as size and weight reduction, in many applications. However the joining of high strength steel must be carried out in a controlled manner, with particular attention placed on welding, if both strength and toughness requirements are to be met.[1–3] Since the 1960s, many investigators have carried out research by varying elemental composition and welding parameters, with the hope of achieving good strength above the region of 690 MPa (100 ksi) and good toughness using shielded metal arc welding.

It was demonstrated in Part 1[4] of this series of papers that the common belief that the toughness of high strength steels and weld metals can be improved by adding nickel is not justified. It was found that whereas nickel increased the strength, it did not lead to an improvement in the impact toughness in alloys containing some 2 wt-% manganese. These experimental observations are consistent with predictions using neural network models. As pointed out in Part 1,[4] the physical basis of this behaviour is that the alloy transforms during cooling into coarse regions of coalesced bainite, which is expected to offer little resistance to cleavage crack propagation. The neural networks predict that this scenario should be different when the nickel concentration is increased but the manganese concentration is decreased; the toughness should then improve at higher nickel contents.

The most promising results to date have been achieved through the variation of manganese and nickel contents.[5–7] Zhang and Farrar[5] investigated a number of compositions with manganese content less than 1·6 wt-% and nickel less than 5·6 wt-%. With a combination of 0·36 wt-%Mn and 5·58 wt-%Ni, an impact toughness of $\sim$55 J at -60°C was recorded and a tensile strength of 904 MPa was predicted from hardness measurements. Increasing manganese content to 0·7 wt-% and reducing nickel to 3·5 wt-% was found to increase impact toughness to $\sim$75 J at -60°C and a reduction in tensile strength to 745 MPa was predicted from hardness measurements. Mainly acicular ferrite with some Widmanstätten sideplates and grain boundary ferrite were reported, whereas increasing nickel content was found to promote martensite.[5] Lord[6]

[1]ESAB AB, PO Box 8004, SE–402 77 Gothenburg, Sweden. Work carried out in the Department of Applied Physics, Chalmers University of Technology, Kemigården 1, Fysikgränd 3, SE–412 96 Gothenburg, Sweden
[2]ESAB AB, PO Box 8004, SE–402 77 Gothenburg, Sweden
[3]Department of Applied Physics, Chalmers University of Technology, Kemigården 1, Fysikgränd 3, SE–412 96 Gothenburg, Sweden
[4]University of Cambridge, Department of Materials Science and Metallurgy, Pembroke Street, Cambridge CB2 3QZ, UK

*Corresponding author, email enda.keehan@esab.se

Published by Maney on behalf of the Institute
Received 7 April 2005; accepted 22 June 2005
DOI 10.1179/174329306X77849

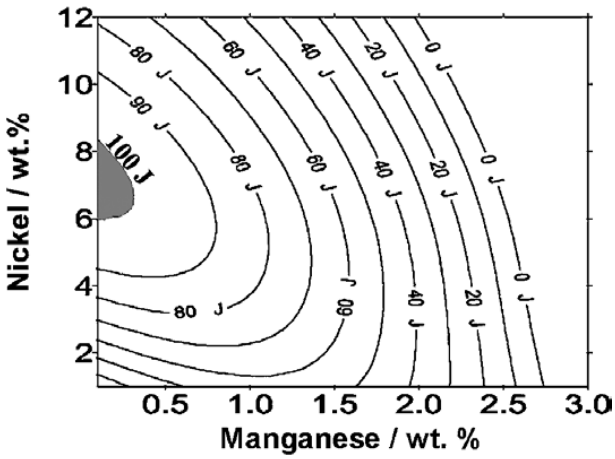

1 Contour plot of impact toughness predictions at −40°C as function of nickel and manganese content for base composition (wt-%) of Fe–0·034C–0·25Si–0·5Cr–0·62Mo (after Ref. 8)

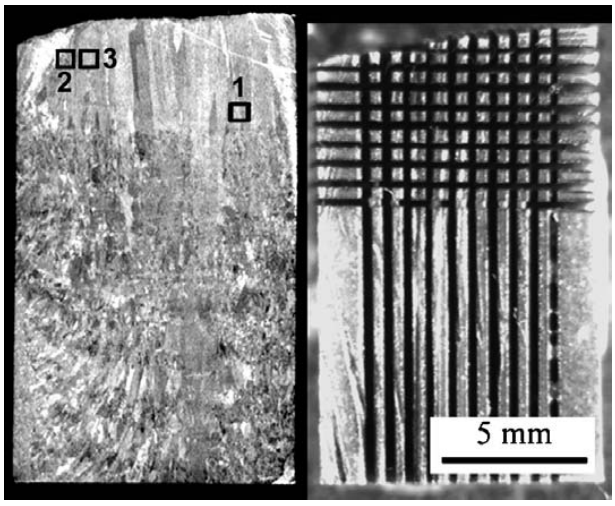

2 Image (LOM) showing block of weld metal from 7–2L250 before and after it was subjected to electric discharge machining: from this image it was possible to locate where rods, and in turn APFIM specimens, were located in relation to individual beads

investigated the effect of nickel additions from 3 to 4 wt-% at decreasing manganese levels from 1·1 to 0·8 wt-% and recorded an impact toughness of up to 74 J at −60°C. Yield strength of 809 MPa was reported for this weld metal.[6] Recently a manganese content of 0·52 wt-% combined with 6·95 wt-%Ni was investigated. An impact toughness of 55 J at −60°C was recorded and yield strength of 684 MPa was predicted for this composition. Microstructural investigations with light optical microscopy (LOM) revealed various forms of ferrite and lath martensite.[7]

These recorded mechanical properties were found to be in close agreement with neural network estimates, where a contour plot suggested that the nickel and manganese concentrations must be optimised as shown in Fig. 1.[8] Based primarily on the neural network predictions, but also on literature, experimental weld metals were produced to study the changes in mechanical and microstructural behaviour in detail for manganese concentrations of 0·5 or 2·0 wt-% and a constant nickel content of 7 wt-%. The present work is the second in a series of three papers that report on the effects of changing nickel,[4] manganese, and carbon[9] content in high strength steel weld metals.

Experimental procedures

The welded joints were produced as described previously.[8] The welding parameters and chemical compositions are presented in Table 1. The weld metals were denoted 7–2L250 and 7–0·5L250 where 7 is the nickel content, 2 or 0·5 is the manganese content, L stands for a low (0·03%) carbon content (all contents are in wt-% throughout unless specified otherwise), and 250 is the interpass temperature in °C. Specimens for Charpy V notch impact testing, tensile testing, dilatometry, and metallographic analysis (using LOM, field emission gun scanning electron microscopy (FEGSEM), and transmission electron microscopy) were prepared as previously described.[8] Secondary ion mass spectroscopy was also carried out on polished specimens in addition to energy dispersive X-ray analysis.

Atom probe field ion microscopy (APFIM) was performed on the last bead of both weld alloys to measure the carbon content of the ferritic matrix. Atom probe specimens were prepared by first removing a block of weld metal, which included the last bead, with approximate dimensions of $10 \times 10 \times 15$ mm. The bead structure of the weld metal was exposed using ammonium peroxidisulphate and photographed. The block was then subjected to electric discharge machining (EDM) using a Charmilles Isopulse type P25 discharge machine. Cuts were made parallel to the welding direction to produce rods with approximate dimensions $0{\cdot}4 \times 0{\cdot}4 \times 10$ mm. On completion of EDM, the sample was again photographed to allow the rod locations to be traced as shown in Fig. 2. Rods were then individually removed and electropolished to produce needle shaped specimens with a tip radius of less than 50 nm using standard electropolishing methods.[11] All specimens were first examined using TEM to observe the shape of the needle, and in some instances the specimen was further electropolished to enhance the specimen shape. This final electropolishing was carried out applying short voltage pulses (10 V for 0·2 to 10 ms) which allows a controllable amount of material to be removed. Once a satisfactory specimen had been obtained, it was investigated at specimen temperatures between 55 and 75 K. The residual gas pressure within the ultrahigh

Table 1 Welding parameters, chemical composition (wt-%, except where stated), and tensile properties

Weld metal	E, kJ mm^{-1}	IPT, °C	$t_{8/5}$, s	C*	Si	Mn	P	S*	Cr	Mo	Ni	Cu	O, ppm*	N, ppm*	YS, MPa	UTS, MPa	YS/UTS	A_5, %
7–2L250	1·2	250	12	0·032	0·25	2·02	0·011	0·008	0·47	0·63	7·23	0·03	380	250	795	1006	0·79	15
7–0·5L250	1	250	10	0·024	0·35	0·64	0·012	0·008	0·21	0·4	6·6	0·03	400	197	721	823·5	0·88	21·3

E energy input; IPT interpass temperature; $t_{8/5}$ estimated cooling time between 800 and 500°C calculated from WeldCalc;[10] YS yield strength; UTS ultimate tensile strength; A_5 elongation.
*Elements analysed using Leco Combustion equipment.

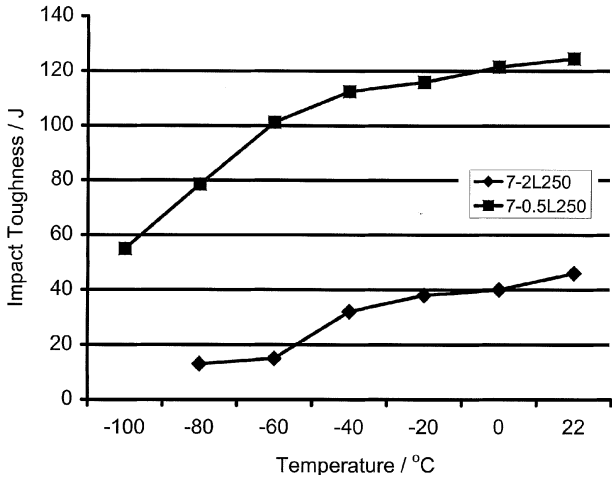

3 Recorded mean Charpy impact toughness as function of temperature

vacuum chamber was kept below 7×10^{-8} Pa and an evaporation pulse amplitude of 20% of the standing voltage was applied. A description of the APFIM instrument and evaluation system may be found elsewhere.[12–14]

Results

Mechanical properties

The recorded tensile properties and Charpy V notch impact toughness levels of the weld metals are presented in Table 1 and Fig. 3, respectively. In short, it was confirmed that reducing manganese content from 2 to 0·5% at 7% nickel leads to a large increase in toughness. As a result of this minor change in composition impact toughness increased from 32 to 113 J at −40°C. With this large increase of toughness, yield strength remained good, with only a moderate decrease from 795 to 721 MPa.

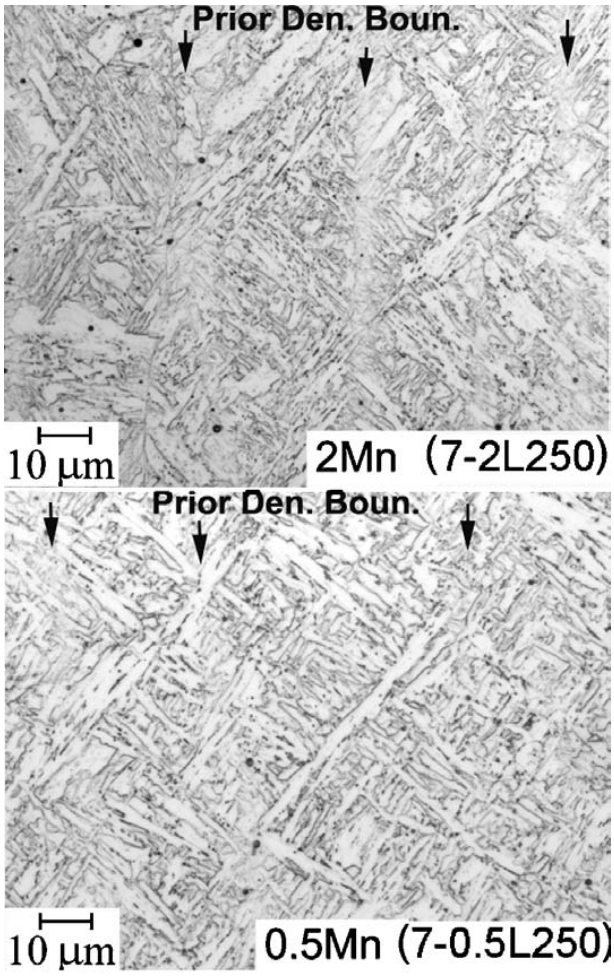

4 Microstructure of as deposited weld metal: effects of segregation during dendritic solidification can be clearly seen (LOM)

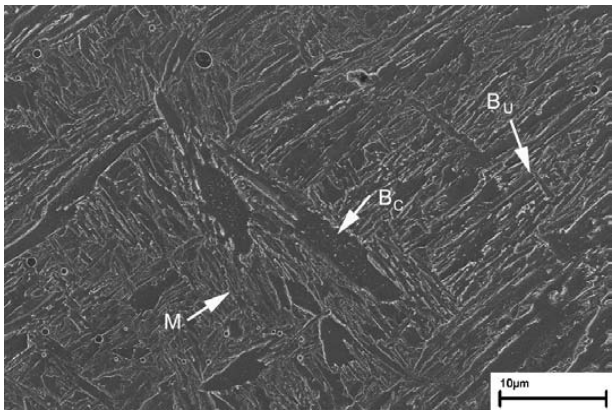

5 Overview (FEGSEM) of microstructure in last bead of 7–2L250: M is martensite, B_U is upper bainite, and B_C is coalesced bainite

Microstructure – last bead

Figure 4 shows LOM images from the last bead of the two weld metals. Thermodynamic calculations presented elsewhere showed that both weld metals solidify as austenite[15] and the resulting dendritic segregation pattern can be clearly seen in Fig. 4. However, without information from high resolution methods it is difficult to state with certainty which microstructural constituents are present.

A representative FEGSEM image from the last bead of weld metal 7–2L250 is shown in Fig. 5. Using FEGSEM it was found that the microstructure was a mixture of upper and lower bainite along with a large grained bainitic constituent within the former dendrites, whereas a lath like microstructure of martensite was predominant at the prior dendrite boundaries. Figure 6 shows cementite precipitates within the large bainitic grains. Previously, extensive examinations of this constituent were carried out with using resolution techniques such as FEGSEM and TEM. It was found that

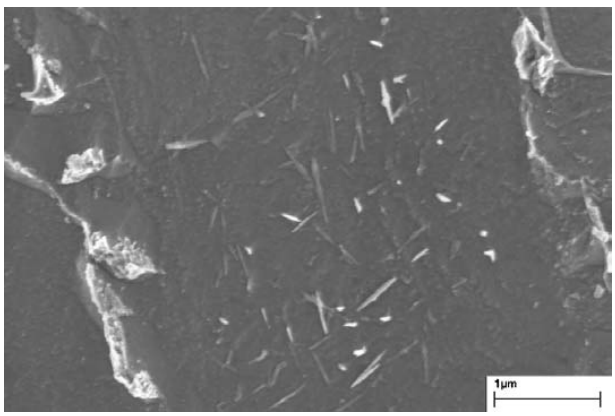

6 Cementite precipitates that form within coalesced bainite in as deposited 2%Mn weld metal (FEGSEM)

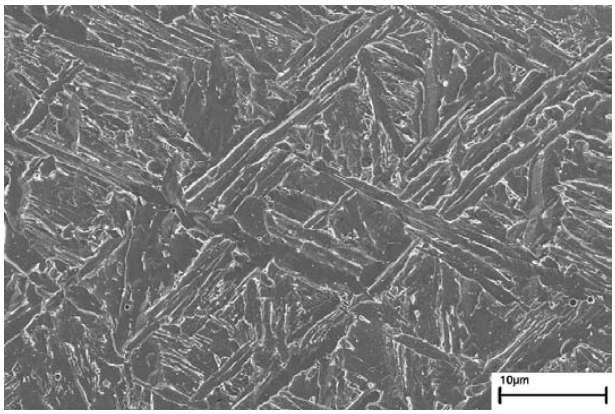

7 Overview of microstructure in last bead of 0·5%Mn weld metal (FEGSEM)

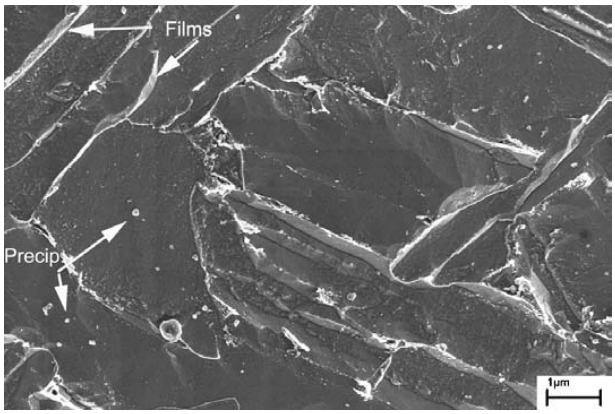

8 Precipitates within grains and films at lath boundaries in last bead of 0·5%Mn weld metal (FEGSEM)

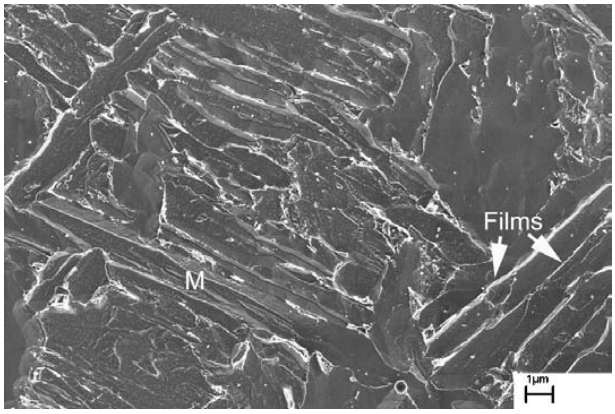

9 Martensite and films at lath boundaries in last bead of 0·5%Mn weld metal (FEGSEM)

very large bainitic ferrite grains formed, without the typical subunit structure of platelets with cementite at boundaries. It was concluded that this constituent was coalesced bainite. Detailed results and discussion may be found elsewhere.[16]

The microstructure of the last bead in the low manganese weld metal was also investigated with FEGSEM (Fig. 7). It was found that the microstructure was mainly upper bainite with some lower bainite. Figure 8 shows a region of relatively coarse bainitic ferrite with some precipitates inside. The precipitates are spherical in nature rather than the lath like precipitates seen in Fig. 6. In both Figs. 8 and 9 films are observed at boundaries, and some martensite can also be seen in Fig. 9.

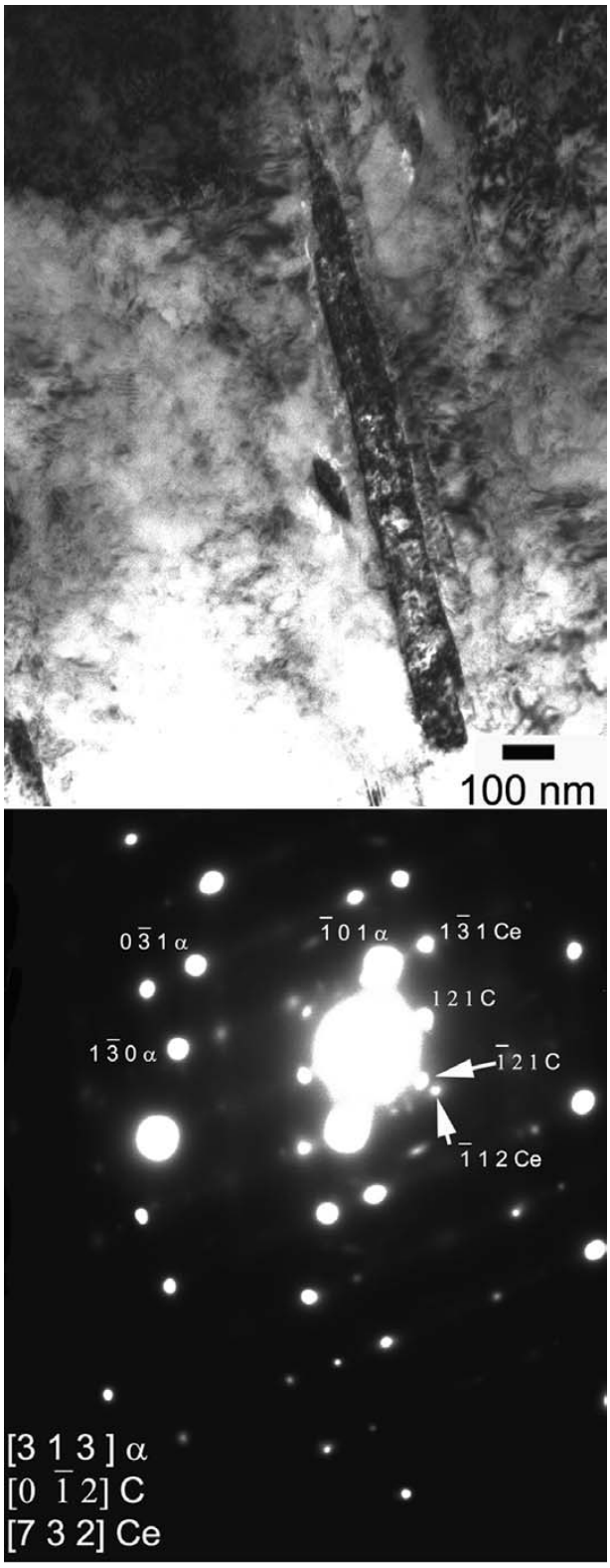

10 *a* TEM bright field image and *b* corresponding selected area diffraction pattern from last bead of 7–2L250: diffraction pattern shows reflections from zone axis $[313]_{\alpha}$ (bainitic ferrite) along with cementite reflections from zone axis $[012]_{C}$ and $[732]_{Ce}$ (subscripts C and Ce represent reflections from two differently orientated families of cementite)

Selected micrographs from TEM investigations on the last bead of 7–2L250 are presented in Figs. 10 and 11. A bright field image is shown together with a

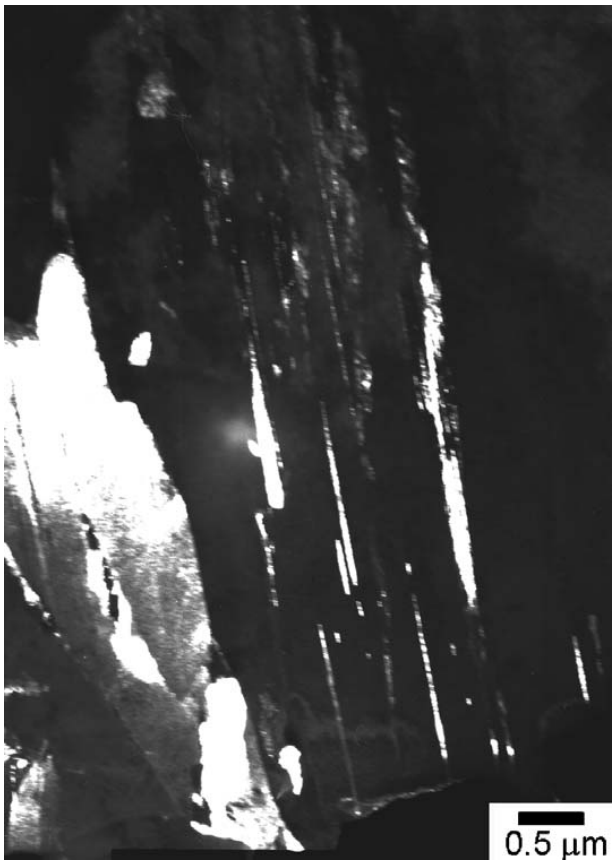

11 Dark field TEM image showing films of cementite at lath boundaries in last bead of 7–2L250: image was formed using $[121]_C$ cementite reflection in selected area electron diffraction pattern shown in Fig. 10

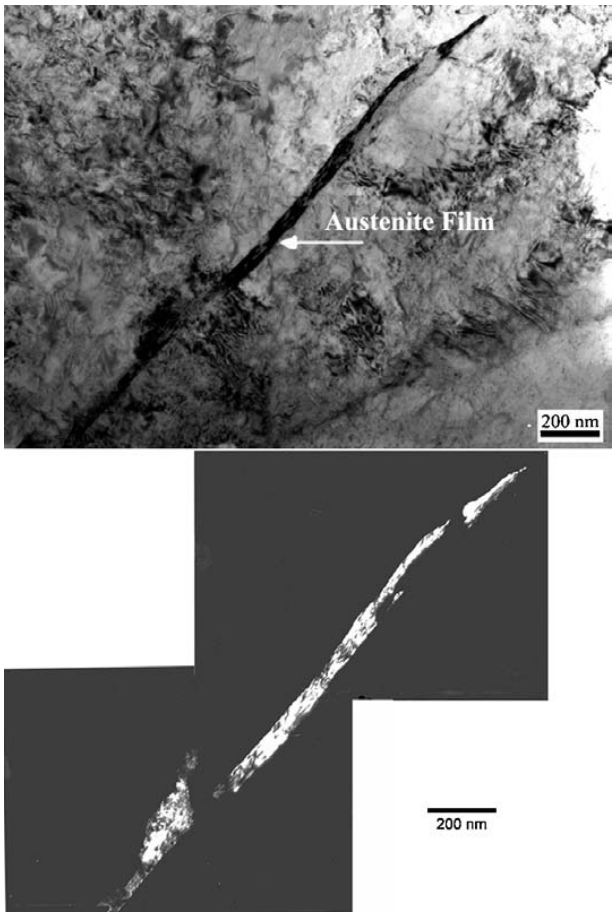

12 Corresponding bright and dark field TEM images showing austenite thin film surrounded by bainitic ferrite in last bead of 7–0·5L250

corresponding selected area diffraction pattern in Fig. 10. The lattice parameters for the individual phases in steel are well known and corresponding distances for allowed reflections are well documented for given camera lengths.[17–19] In the diffraction pattern, reflections were found that correspond to ferrite or cementite. When a cementite spot was selected to form a dark field image the black film in the bright field image was illuminated. Reducing the magnification in the dark field mode allows the distribution of cementite to be observed as shown in Fig. 11. From this analysis it was concluded that upper bainite was formed within the microstructure and this allows the identification of upper bainite in the FEGSEM image shown in Fig. 5. Further investigations on this weld metal using TEM, in which coalesced bainite is characterised, are presented and discussed elsewhere.[16] Limited investigations with TEM on as deposited weld metal from 7–0·5L250 were carried out. Bright and dark field images are shown in Fig. 12, where a film of retained austenite was characterised using electron diffraction.

Investigations using APFIM were carried out to measure carbon content in the ferritic phase. Different regions within the last bead of both the 2 and 0·5% manganese weld metals were analysed and the results of three runs from each are presented in Table 2. The carbon content recorded in the first run with the 2%Mn weld metal was very low in comparison with the nominal level of 0·03%. The nickel and manganese contents were also slightly lower than the nominal level and it is suggested that the sample was from a dendrite core region. The other two runs have much higher carbon contents, comparable to the nominal level. For these runs it was found that nickel and manganese levels were higher than the nominal levels, suggesting interdendritic regions. Carbon content was similar to the nominal level for all runs in the 0·5%Mn weld metal. However,

Table 2 Atom probe field ion microscopy (APFIM) results, showing average levels of carbon, manganese, and nickel (wt-%$\pm\sigma$) from individual APFIM runs along with number of ions collected: most likely constituent as deduced from composition is indicated, where B is bainite and M is martensite

Weld metal	Ions	C	Mn	Ni	Constituent
7–2L250	34540	0·007±0·002	1·89±0·07	7·06±0·29	B
	4286	0·025±0·011	2·27±0·23	7·63±0·78	M
	4661	0·055±0·016	2·54±0·23	7·63±0·81	M
7–0·5L250	5034	0·034±0·012	0·59±0·17	7·14±0·75	M
	72235	0·022±0·003	0·46±0·02	5·98±0·18	M
	73389	0·027±0·003	0·54±0·03	6·85±0·19	M

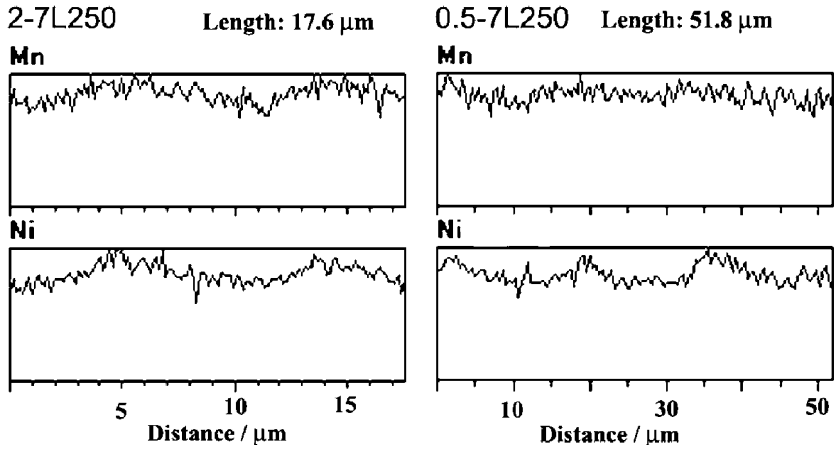

13 Elemental line scans (EDX) across former dendrites in last bead, showing segregation of nickel and manganese: dendrite boundary regions are indicated with broken lines, and *y* axis shows relative intensity measured

manganese content was lower than the nominal levels in all runs whereas nickel was slightly higher, with the exception of the second run where a significant depletion was seen.

Elemental distribution

When the last bead was investigated using SEM in the backscattered mode, a clear contrast was seen between the dendrite boundaries and the centres on polished samples. Elemental line scans were therefore carried out across the dendrites using EDX. The results are presented in Fig. 13 and it can be seen that the concentrations follow a wavelike pattern with enrichment of nickel and manganese at the former dendrite boundary regions. EDX spot analysis was used to quantify the degree of segregation (Table 3). There is a slight overestimation of the manganese concentration but the results nevertheless allow an estimate of the degree of segregation between the dendrite boundaries and the centres. Segregation of manganese is less for the lower alloying content of 0·5%, whereas the difference in nickel concentration is almost the same in both the weld metals.

SIMS was employed to allow the elemental segregation over a given area to be mapped; results from the last bead are presented in Fig. 14. In each image, regions where the individual element is concentrated appear brighter in contrast. It can be seen that manganese is segregated to manganese rich inclusions and to interdendritic regions whereas nickel was found to segregate to interdendritic regions. Overall, the results were in agreement with those obtained from EDX analysis.

Microstructure – reheated beads

In regions reheated by multiple weld passes it was still possible to distinguish the former dendrites using FEGSEM (Fig. 15). It was found that some precipitates had coarsened while other new small precipitates formed and that carbon had redistributed within the bainitic ferrite in the centre of dendrites. The lath like precipitates were replaced by some larger and numerous small spherical precipitates within the bainitic ferrite plates, whereas more elongated precipitates were found at the plate boundaries (Fig. 16). A tempered martensitic microstructure was found in interdendritic regions as shown in Fig. 17.

Table 3 Average compositions (wt-%) at dendrite boundary regions and dendrite core regions in last bead, obtained using EDX spot analysis

Weld metal	Region	Mn	Ni
7–2L250	Boundary	3·10	8·18
	Core	2·35	6·30
	Difference	0·75	1·88
7–0·5L250	Boundary	0·95	7·55
	Core	0·57	5·83
	Difference	0·38	1·72

Selected micrographs are presented in Figs. 18 and 19 for 7–0·5L250. Figure 18 shows an overview of the microstructure and again the dendritic structure is clearly visible. As in the high manganese weld metal it was found that carbon redistributed within bainitic ferrite in the dendrite core regions as shown in Fig. 19. Precipitates were found both within the grains and at the grain boundaries. At interdendritic regions a tempered martensitic microstructure was found.

Reheated regions of both weld metals were also investigated using TEM. A bright field and corresponding dark field image from the 2%Mn weld metal are presented in Fig. 20. A bainitic ferrite grain boundary region is shown and elongated precipitates can be seen at the boundary in the bright field mode. When the dark field image was formed using a cementite reflection from the selected area diffraction pattern, elongated precipitates at the boundary and small precipitates within the grains appeared bright. The observed precipitates have a similar morphology to those examined using FEGSEM as shown in Fig. 16. A bright field image of a grain in a reheated bead of the 0·5%Mn weld metal is shown in Fig. 21. This grain was investigated at higher magnifications and found to contain cementite precipitates. A selected area diffraction pattern with a corresponding dark field image of cementite is shown in Fig. 22. The dark field image was formed using a cementite reflection. These precipitates are similar in morphology to the precipitates found within the bainitic ferrite grains using FEGSEM in Figs. 16 and 19.

Dilatometry

Phase transformation temperatures were measured using dilatometry. The Ac_1 and Ac_3 temperatures were measured to be 700 and 770°C, respectively, for 7–0·5L250 when samples were heated at a rate of 25 K s^{-1}.

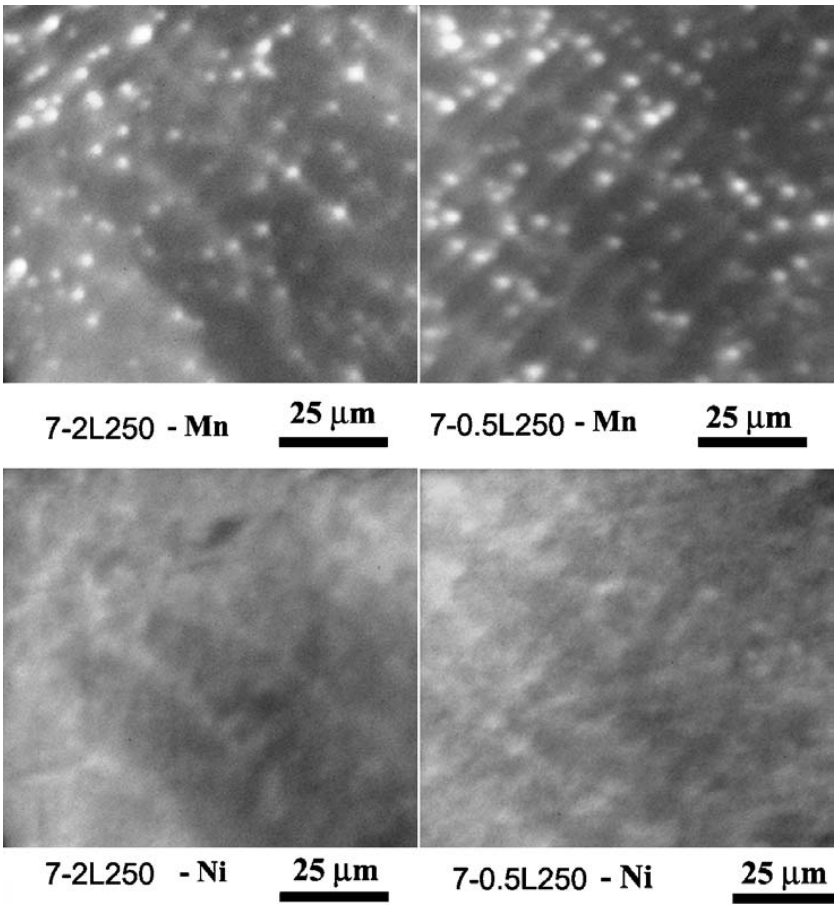

14 Segregation of nickel and manganese to dendrite boundaries in last bead of 7–2L250 and 7–0·5L250 (SIMS): areas where given element is concentrated appear brighter in contrast (imaging of elements was carried out using O_2^+ primary ions)

These temperatures can be compared with 690 and 740°C for Ac_1 and Ac_3 for the high manganese weld metal.

On cooling it was found that austenite began to transform in the region of 490°C when cooled at a rate of approximately 40 K s^{-1} and at 480°C when cooled at 1 K s^{-1} for the 0·5%Mn weld metal. These values can be compared with 373°C and 390°C for the 2·0%Mn weld metal when samples were cooled at a rate of 25 K s^{-1} and 1 K s^{-1}, respectively.

Discussion

Both experimental weld metals were composed of martensite and different forms of bainite along with small amounts of retained austenite (*see* Fig. 12 and Ref. 7). Although broadly the same constituents were found, reducing manganese content from 2 to 0·5% promoted noticeable differences in the weld metal microstructure and properties.

Microstructure

In both alloys, EDX and SIMS measurements showed that manganese and nickel segregate to interdendritic regions as the weld metal solidifies. As expected, dilatometry showed that austenite was stabilised to lower transformation temperatures for richer manganese

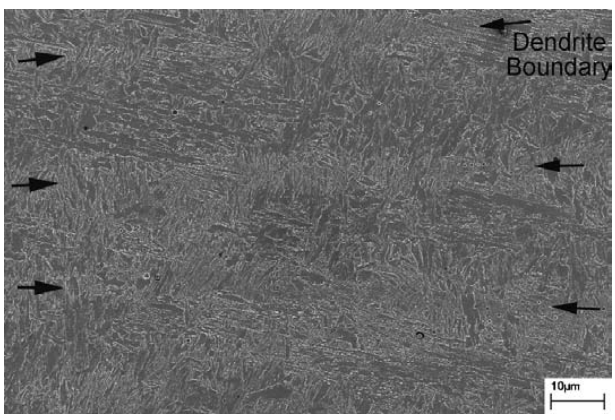

15 Centre of reheated bead in 7–2L250, clearly showing former dendrites (FEGSEM)

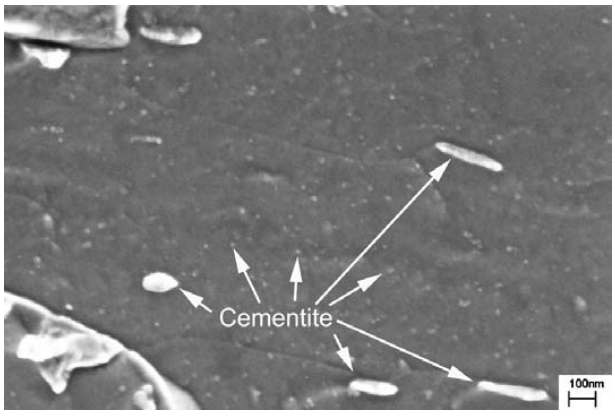

16 High magnification FEGSEM image of cementite precipitates in central regions of former dendrite in reheated bead of weld metal 7–2L250

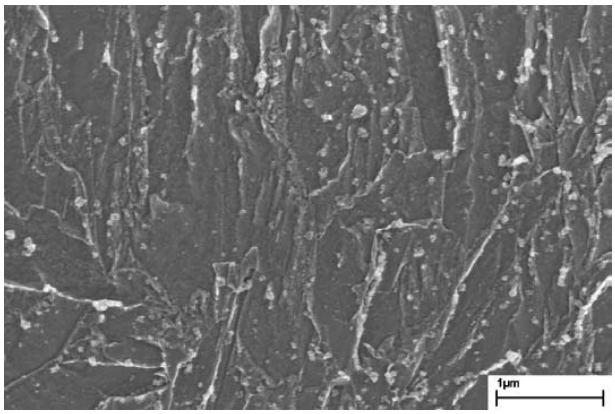

17 Former interdendritic region in reheated bead of 7–2L250 weld metal, showing mainly tempered martensite (FEGSEM)

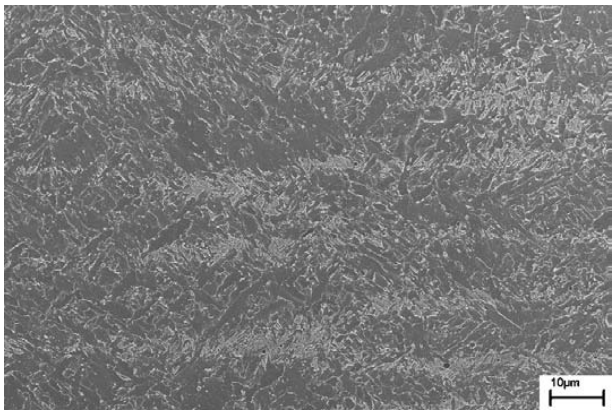

18 Low magnification FEGSEM image showing overview of microstructure in centre of reheated bead in weld metal 7–0·5L250

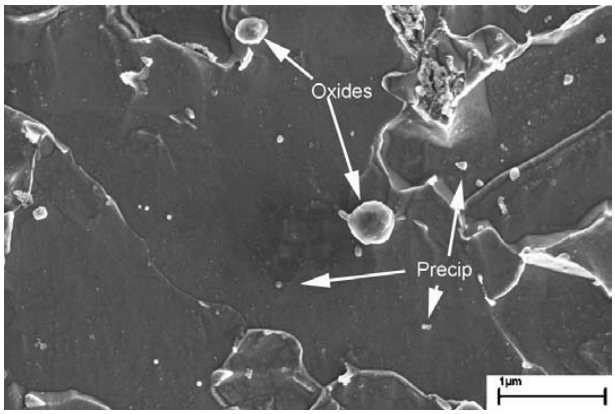

19 Precipitates in central regions of former dendrite in reheated bead of weld metal 7–0·5L250 shown at high magnification (FEGSEM)

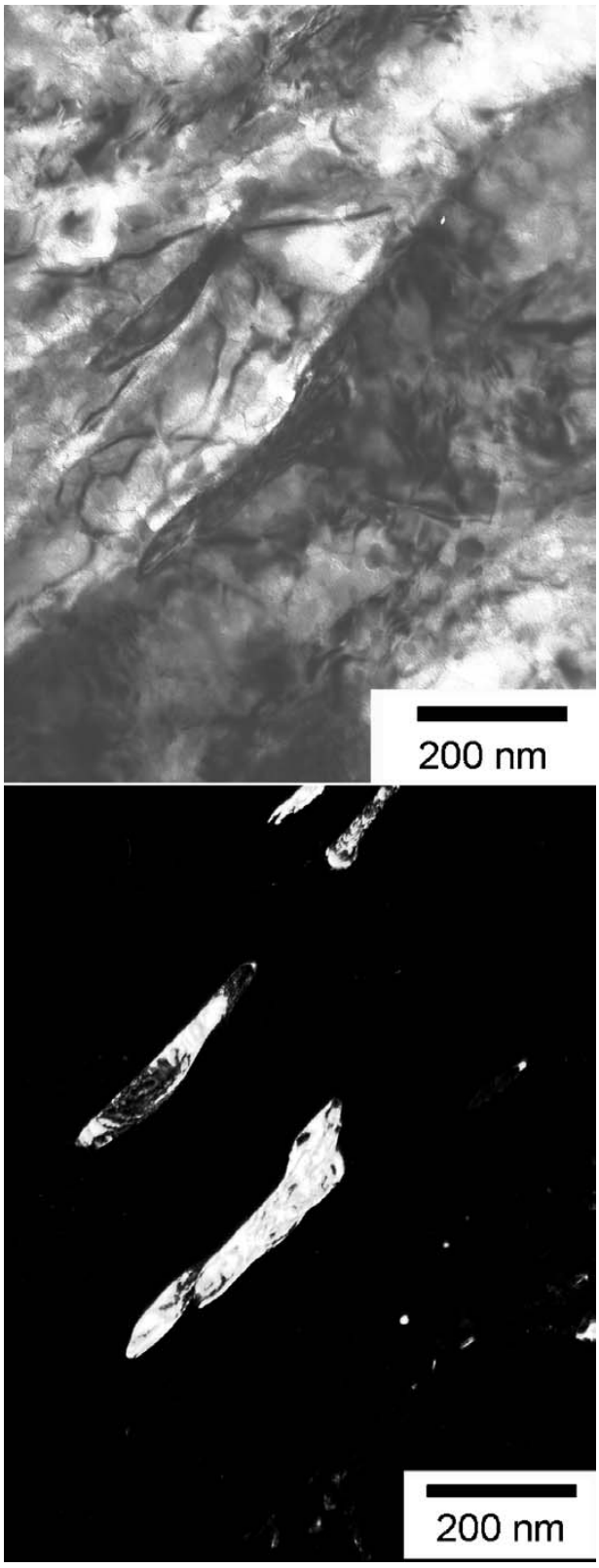

20 *a* TEM bright field image with *b* corresponding dark field image, showing cementite precipitates in reheated bead of 7–2L250 weld metal

contents and a difference of about 100 K was recorded between the 0·5 and 2·0%Mn steels. Similarly, the transformation temperature decreased by 10–30 K when the nickel content was increased from 7 to 9% at 2%Mn as is presented elsewhere.[4] This is in agreement with more of the low transformation constituents martensite and coalesced bainite forming in the 2%Mn weld metal, rather than upper bainite which forms at higher temperatures. It also explains why martensite was found mainly in former interdendritic regions where alloying content was richer.

From FEGSEM and TEM studies it was evident that mainly upper bainite formed in the 0·5%Mn weld metal (Fig. 7), whereas significant amounts of coarse grained coalesced bainite and martensite are present in the

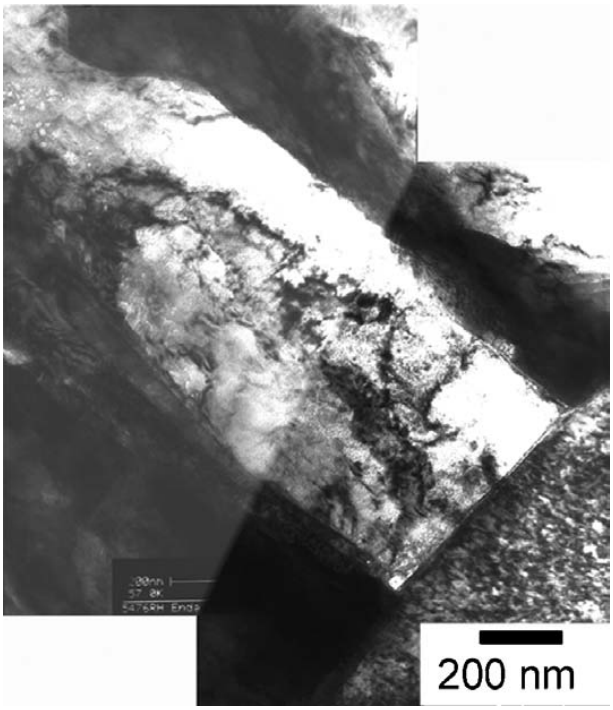

21 Bright field TEM image of grain in reheated bead of 7–0·5L250 weld metal

2%Mn metal. Furthermore, using APFIM it proved possible to measure the local carbon content and to distinguish between martensite and bainite. These measurements reaffirmed FEGSEM and TEM results that both constituents are present in the 2%Mn steel and also that small amounts of martensite were present at 0·5%Mn. Numerous cementite precipitates were formed within the bainitic ferrite grains in the 2%Mn material (Fig. 6) whereas fewer precipitates were developed at 0·5%Mn (Fig. 8). This is in agreement with the observation that the bainitic ferrite grains are smaller in the 0·5%Mn weld metal, resulting in shorter diffusion distances to boundaries. Carbon also has a greater mobility at the higher transformation temperature measured for 0·5%Mn. Additionally, thermodynamic calculations[20] show that manganese is a strong cementite stabiliser and that greater amounts of precipitates are therefore likely to develop in the 2%Mn weld metal.

Mechanical properties

Since mechanical properties are recorded in reheated regions it is necessary to understand the tempered microstructure. It was found that Ac_1 and Ac_3 were slightly reduced with high manganese content and it follows that a greater proportion of the underlying beads was transformed back to austenite on the deposition of new weld metal. In both weld metals tempered martensite was the main microstructure at the interdendritic regions whereas generally tempered bainite was present at dendrite core regions. Cementite was observed in the form of elongated films at bainitic ferrite plate boundaries and as precipitates within the plates in the 0·5%Mn weld metal. In the high manganese weld metal it was found that carbon was redistributed in the bainitic ferrite with cementite coarsening and spheroidising. Numerous very small precipitates (Fig. 16) were

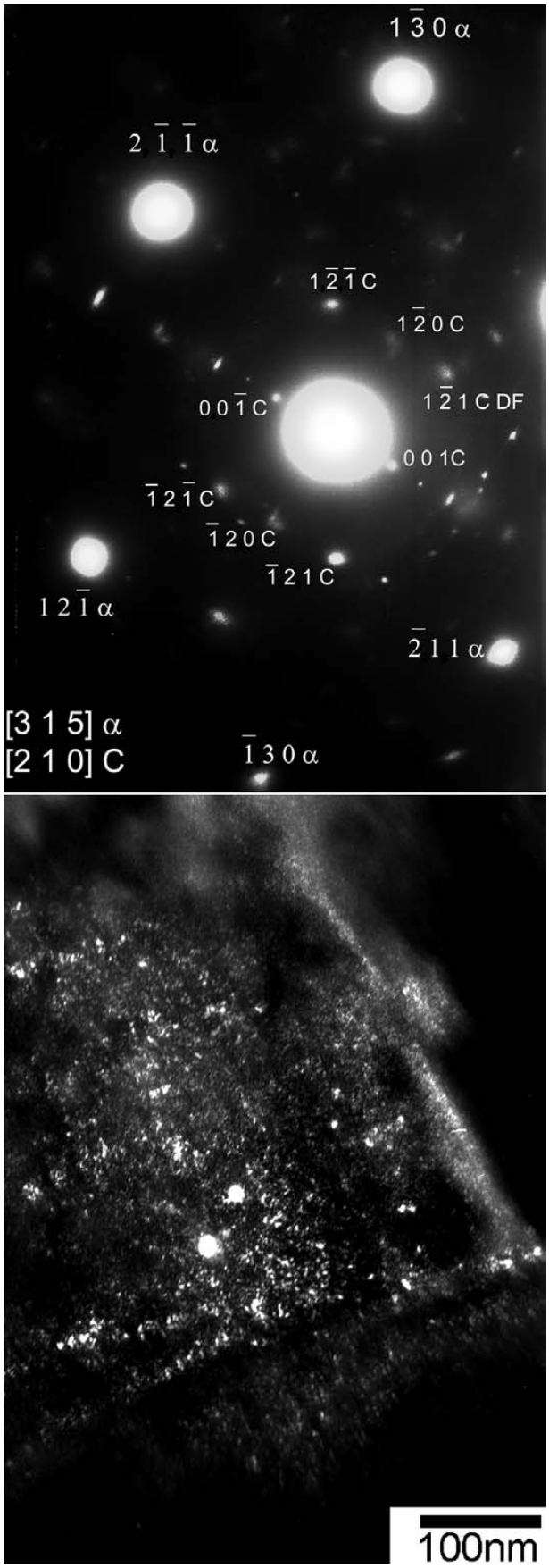

22 Selected area diffraction pattern from grain shown in Fig. 21 with corresponding dark field image showing small cementite precipitates in reheated bead of 7–0·5L250: dark field image was formed using the $[121]_C$ cementite reflection (TEM)

also found and it is thought that these were newly formed from the carbon dissolved in the matrix on tempering.

The poor toughness associated with the 2%Mn weld metal was attributed to the larger grain size of the coalesced bainite, which is thought to offer little resistance to cleavage crack propagation. Also, from dilatometry measurements it can be concluded that less tempering and more reaustenitisation occurs within the 2%Mn weld metal as a result of lower Ac_1 and Ac_3 temperatures. This contributes to greater amounts of less tempered microstructure. In the 0·5%Mn weld metal, upper bainite with a smaller grain size was dominant within the microstructure. This weld metal also experienced more tempering since Ac temperatures were higher.

Conclusions

For the two 7 wt-% nickel experimental weld metals produced, it was found that reducing manganese content from 2 to 0·5 wt-% leads to a large increase in impact toughness with only a moderate reduction in strength.

High resolution investigations confirmed that the microstructure was a mixture of martensite, coalesced bainite, and upper bainite along with some retained austenite. Upper bainite was the dominant microstructural constituent in the 0·5%Mn weld metal, whereas coalesced bainite and martensite were the major constituents in the 2%Mn weld metal. Microstructural observations were in agreement with dilatometry experiments, where manganese was found to stabilise austenite on cooling.

Using EDX and SIMS it was observed and quantified that manganese and nickel segregated to former interdendritic regions, leaving a leaner alloying content within the core of the former dendrites. These segregation patterns result in greater amounts of martensite in former interdendritic regions, where the greater solute content causes the austenite to transform at lower temperatures. Conversely, bainite formed at higher temperatures within the dendrites owing to the leaner alloying content.

It was concluded that the lower impact toughness in the 2%Mn weld metal was largely due to the large grain size of coalesced bainite. Good toughness in the 0·5%Mn weld metal was attributed to a finer grain size and the occurrence of greater amounts of tempering.

Acknowledgements

Professor L.-E. Svensson of Chalmers University of Technology and Dr M. Thuvander of ESAB AB are thanked for fruitful discussions. Mr P. Lindström of Sandvik Technology is gratefully acknowledged for help with dilatometry experiments. ESAB AB is thanked for the production of experimental weld metals, permission to publish results, and financial support. The Knowledge Foundation of Sweden is thanked for additional financial support.

References

1. L.-E. Svensson: *Svetsaren*, 1999, **54**, 29.
2. J. J. Deloach, C. Null, S. Fiore and P. Konkol: *Weld. J.*, 1999, **78**, (6), 55–58.
3. D. J. Widgery, L. Karlsson, M. Murugananth and E. Keehan: 'Approaches to the development of high strength weld metals', Proc. 2nd Int. Symp. on 'High strength steel', Verdal, Norway, April 2002, SINTEF Materials Technology.
4. E. Keehan, L. Karlsson and H. O. Andrén: *Sci. Technol. Weld. Joining*, 2006, **11**, (1), 1–8.
5. Z. Zhang and R. A. Farrar: *Weld. J.*, 1997, **76**, (5) 183s–196s.
6. M. Lord: 'Design and modelling of ultra-high strength steel weld deposits', PhD thesis, University of Cambridge, Cambridge, UK, 1999.
7. Y. Kang, H. J. Kim and S. K. Hwang: *ISIJ Int.*, December 2000, **40**, 1237.
8. M. Murugananth, H. K. D. H. Bhadeshia, E. Keehan, H. O. Andrén and l. Karlsson: 'Strong and tough ferritic steel welds', in 'Mathematical modelling of weld phenomena 6' (ed. H. Cerjak), 205–230; 2002, Abington, UK, Woodhead.
9. E. Keehan, L. Karlsson, H. O. Andrén and H. K. D. H. Bhadeshia: *Sci. Technol. Weld. Joining*, 2006, **11**, (1), 19–24.
10. 'WeldCalc' software, Version 1.0.0, SSAB, Oxelösund, Sweden, 1998–1999.
11. M. K. Miller, A. Cerezo, M. G. Hetherington and G. D. W. Smith: 'Atom probe field ion microscopy', 483; 1996, Oxford, UK, Clarendon Press.
12. H. O. Andrén and H. Norden: *Scand. J. Metall.*, 1979, **8**, 147.
13. H. O. Andrén: *J. Phys.*, 1986, **47**, (C7), 483.
14. U. Rolander and H. O. Andrén: *J. Phys.*, 1989, **50**, (C8), 529.
15. E. Keehan: PhD thesis, Paper 8, Chalmers University of Technology, Gothenburg, Sweden, 2004.
16. E. Keehan: PhD thesis, Paper 3, Chalmers University of Technology, Gothenburg, Sweden, 2004.
17. K. W. Andrews, D. J. Dyson and S. R. Keown: 'Interpretation of electron diffraction patterns', 2nd edn; 1971, London, Adam Hilger.
18. J. W. Edington: 'Practical electron microscopy in material science', 118; 1975, London, The Macmillan Press.
19. Internet http://cimesg1.epfl.ch/CIOL/ems.html, Centre Interdisciplinaire de Microscopie Electronique, Ecole Polytechnique Fédérale de Lausanne, Lausanne, France.
20. Thermodynamic model, version 4.73 For LNX RH 7·3, NPL Materials Centre, National Physical Laboratory, Teddington, November 2002.